Reconstitution of Contractile Actomyosin Bundles

Todd Thoresen,[†] Martin Lenz,[†‡] and Margaret L. Gardel[†‡*]
[†]Institute for Biophysical Dynamics and [‡]James Franck Institute and Department of Physics, University of Chicago, Chicago, Illinois

ABSTRACT Contractile actomyosin bundles are critical for numerous aspects of muscle and nonmuscle cell physiology. Due to the varying composition and structure of actomyosin bundles in vivo, the minimal requirements for their contraction remain unclear. Here, we demonstrate that actin filaments and filaments of smooth muscle myosin motors can self-assemble into bundles with contractile elements that efficiently transmit actomyosin forces to cellular length scales. The contractile and force-generating potential of these minimal actomyosin bundles is sharply sensitive to the myosin density. Above a critical myosin density, these bundles are contractile and generate large tensile forces. Below this threshold, insufficient cross-linking of F-actin by myosin thick filaments prevents efficient force transmission and can result in rapid bundle disintegration. For contractile bundles, the rate of contraction decreases as forces build and stalls under loads of ~0.5 nN. The dependence of contraction speed and stall force on bundle length is consistent with bundle contraction occurring by several contractile elements connected in series. Thus, contraction in reconstituted actomyosin bundles captures essential biophysical characteristics of myofibrils while lacking numerous molecular constituents and structural signatures of sarcomeres. These results provide insight into nonsarcomeric mechanisms of actomyosin contraction found in smooth muscle and nonmuscle cells.

INTRODUCTION

Thick filaments of myosin motors and filamentous actin (F-actin) form the basis of the actomyosin cytoskeleton, which is essential for contraction and force generation in nonmuscle and muscle cells (1–4). Actomyosin networks and bundles of varied compositions and structures are used in diverse physiological processes including muscle contraction (4,5), cell migration (6,7), and cell division (8,9). Significant progress has been made in understanding the mechanisms of force generation and translocation at the scale of individual myosin motors (10,11). However, knowledge of how actomyosin interactions at the molecular level are transmitted to cellular length scales is essential for developing physical models of cellular mechanics.

In striated muscle, force transmission from the molecular to tissue level is well understood (11–14). Within these tissues, myofibrils consist of a series of contractile elements, termed sarcomeres, which form a well-defined, periodic structure on micrometer length scales (12,15). Sarcomeres consist of bipolar myosin thick filaments bound to F-actin of organized polarity and uniform length. The F-actin pointed ends are oriented toward the central bare zone of the thick filament such that motor-mediated F-actin translocation results in contraction, as described by the sliding filament theory (16). At the F-actin barbed ends, passive cross-linking proteins (e.g., α-actinin) serve to link sarcomeres in series (12,15). The exquisite organization of sarcomeres has facilitated our understanding of force transmission in striated muscle. However, there are numerous types of contractile actomyosin bundles in smooth and nonmuscle cells that lack sarcomeric organization (7,9,17–19). In these nonsarcomeric actomyosin bundles, the underlying mechanisms of contraction and the roles of passive cross-linking proteins are not well understood.

Contraction of actomyosin assemblies in vitro is traditionally studied by polymerizing F-actin in the presence of myosin thick filaments and then assessing the extent of network contraction and force generation at length scales ranging from 100 μm to 10 cm (20–26). Although early work indicated that mixtures of highly concentrated F-actin and myosin contract and generate force (21), it was later shown that these behaviors were not consistent with myosin mechanochemistry and were likely dominated by contaminating factors (27). More recent experiments indicate that passive F-actin cross-linking proteins, such as α-actinin or filamin, are required to facilitate network contraction (23–26). Thus, it is widely believed that myosin filaments alone are insufficient to elicit contraction of actin bundles on cellular length scales.

Contrary to these expectations, we show that a high density of smooth muscle myosin thick filaments is sufficient to elicit contraction of actomyosin bundles in the absence of passive cross-linking proteins. As the myosin density is decreased, we observe first a regime where F-actin bundles are stabilized by myosin cross-links, but no contraction occurs. When myosin density is decreased further, actin bundles are unstable. In contractile bundles, the rate of contraction is load dependent and stalls under forces of ~0.5 nN. This stall force is independent of bundle length. Under low loads, the contraction rate is proportional to bundle length and increases with the density of myosin filaments. These data are consistent with bundle contraction occurring by a series of independent contractile elements. Thus, bundles comprised solely of myosin thick filaments and F-actin spontaneously assemble into linear arrays of

Submitted November 12, 2010, and accepted for publication April 13, 2011.

*Correspondence: gardel@uchicago.edu

Editor: Christopher Lewis Berger.

0006-3495/11/06/2698/8 $2.00

doi: 10.1016/j.bpj.2011.04.031

contractile elements that capture the essential biophysical properties of striated myofibrils, although lacking their apparent microstructure and many of their components.

RESULTS

Templated assembly of tethered actomyosin bundles

To template assembly of tethered actomyosin bundles, F-actin asters are formed by decorating neutravidin beads bound to a coverslip with biotinylated, Alexa 568-phalloidin-stabilized F-actin with a mean length of ~6 μm (Fig. 1, *a* and *b*, see also Fig. S3, *a* and *b*, and Movie S1 in the Supporting Material). Because biotinylated actin is randomly incorporated into F-actin, free F-actin ends emanating from beads (*asterisks*, Fig. 1 *b*) are likely of random polarity. A dilute background of free F-actin remains after wash steps.

Thick filaments of Oregon Green (OG)-labeled, smooth muscle myosin with a mean length of ~360 nm are prepared (Fig. S1 and Fig. S3, *d* and *e*), diluted in Assay Buffer and perfused into the flow chamber (Fig. 1 *a*). Because the Assay Buffer contains no nucleotides (NN), the myosin heads are bound with high affinity to F-actin either in rigor or with ADP (28). Over a period of 30 min, actomyosin bundles form (Fig. 1 *c*, Fig. S2 *d*, Movie S2). Bundles are largely confined to the coverslip vicinity and elevated from the surface by ~2–4 μm (Fig. S2 *e*). After bundle formation, myosin remaining in solution is removed by perfusion of Assay Buffer.

The bundle lengths vary widely from 5 to >50 μm, significantly longer than individual F-actin, indicating that F-actin in solution is used to assemble bundles. Bundles often branch and connections between bundles can exist far away from the beads (Fig. 1 *c*). The variations of both myosin and actin intensity along the bundle contour are, on average, 10% that of the mean intensity (Fig. 1 *d*). Thus, there are no periodic myosin bands indicating sarcomeric organization (29) within the bundle. Using quantitative fluorescence microscopy, we estimate ~4 F-actin per bundle cross section (Fig. 1 *e*).

The bundle composition can be altered by varying the myosin concentration from 0.1 μM to 1 μM. Strikingly, the number of F-actin per bundle cross section is independent of myosin concentration (Fig. 1 *e*). Using quantitative fluorescence microscopy (Fig. S4), we determine that the mole ratio of myosin heavy chains to actin within bundles, $R_{M:A}$, changes from 0.03 to ~2 for bundles formed with 0.1 μM and 1 μM myosin, respectively (Fig. 1 *f*). Values of $R_{M:A}$ obtained from imaging are consistent with those obtained from densitometry measurements (Fig. 1 *f*). Because the quantity of actin within bundles does not change, $R_{M:A}$ is also a good measure of the absolute density of myosin per bundle length.

Bundles within a large range of $R_{M:A}$ (0.44–1.9) have qualitatively similar morphologies in the presence of Assay Buffer (*top row*, Fig. 2 *a*). They are curved, branched, and fluctuate significantly. For bundles tethered at both ends, the variance of the bundle position in the transverse direction, u_{peak}, (Fig. 1 *d*) provides a measure of the degree of bundle flexibility and does not change significantly as

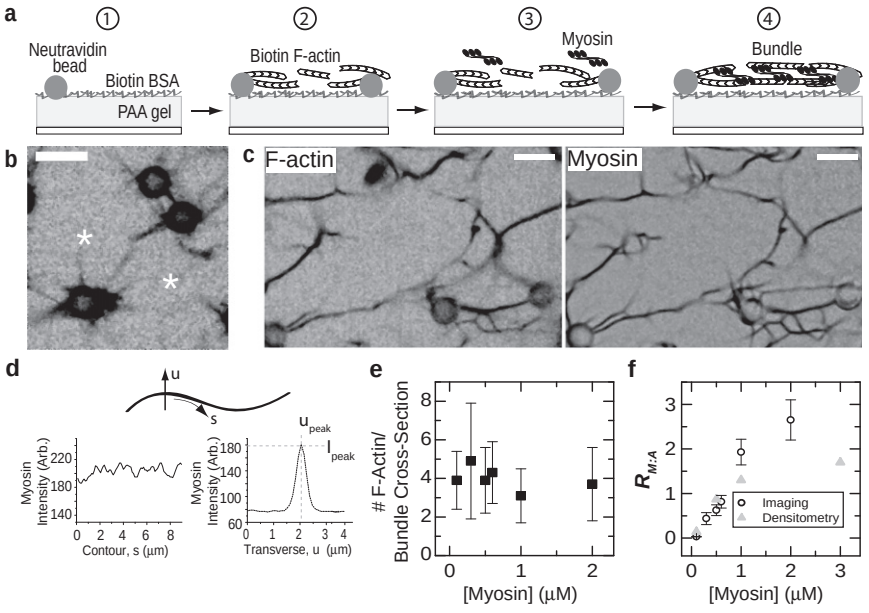

FIGURE 1 Templated assembly of tethered actomyosin bundles. (*a*) Schematic illustrating the sequential process used for templated bundle assembly (*1*). Biotinylated-bovine serum albumin is coupled to the surface of a PAA gel affixed to a glass coverslip. Neutravidin beads (*gray circles*) bind to the biotinylated-bovine serum albumin (*2*). Biotinylated F-actin (*chevrons*) is introduced and bind to beads. A dilute suspension of F-actin remains (*3*). Myosin thick filaments suspended in nucleotide free Assay buffer (*black*) are introduced (*4*). F-actin cross-linking by myosin filaments mediates bundle formation. (*b*) Inverted contrast image of F-actin asters visualized with Alexa 568-phalloidin before myosin perfusion. Dark circles are F-actin-coated beads. Asterisks indicate free F-actin ends. Scale bar is 5 μm; see Movie S1. (*c*) Inverted contrast images of F-actin visualized with Alexa 568-phalloidin (*left*) and OG-labeled myosin (*right*) illustrating network of bundles formed after 30 min incubation of F-actin asters with myosin thick filaments. Scale bar is 5 μm. (*d*) Schematic diagram illustrating transverse, *u*, and longitudinal, *s*, directions along a bundle. Plots of OG-myosin intensities in transverse and longitudinal line scans are shown below. For transverse line scans, the location, u_{peak}, and intensity, I_{peak}, of the peak are determined. (*e*) Number of F-actin per bundle cross section as a function of myosin concentration. Error bars indicate standard deviations, (n = 7–28 bundles for each data point). (*f*) The mole ratio of myosin heavy chains to actin in the bundles determined from quantitative fluorescence imaging (*triangles*) and densitometry (*open circles*) as a function of myosin concentration. Error bars for imaging indicate standard error (n = 20 bundles for each data point).

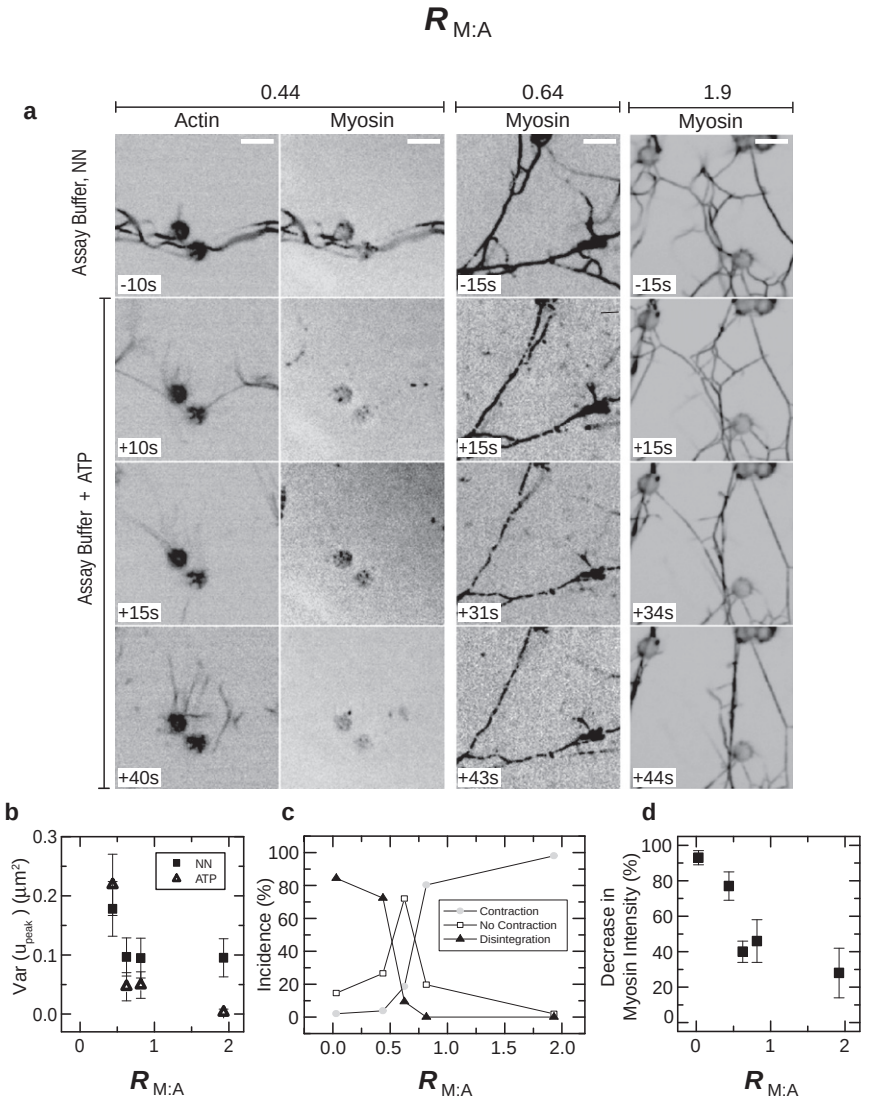

FIGURE 2 A critical myosin density is required to stabilize bundles and facilitate contraction. (*a*) Inverted contrast images of OG-myosin in bundles formed with $R_{M:A} = 0.44$, 0.64 and 1.9 in nucleotide-free (NN) Assay buffer (*top row*) and at three times after addition of Assay buffer containing 1 mM ($R_{M:A} = 0.44$ or 0.64) or 0.1 mM ($R_{M:A} = 1.9$) ATP (*bottom rows*). All times are indicated in seconds either before (*negative times*) or after (*positive times*) ATP addition. For $R_{M:A} = 0.44$, inverted contrast images of F-actin, visualized with Alexa 568-phalloidin, is also shown to illustrate the dissociation of F-actin from bundles and the reappearance of F-actin asters by +40s (see Movie S3). Scale bars are 5 μm. (*b*) Amplitude of transverse fluctuations of bundle contour, measured by the variance of the bundle midpoint position in direction normal to the bundle contour, u_{peak}, as a function of $R_{M:A}$ in both nucleotide-free (*solid black squares*, NN) or 1 mM ATP (*open triangles*, ATP) conditions. Data shown are mean ± SE. ($n =$ 12–15 bundles for all conditions). (*c*) Incidence, reported as percentage, of the states observed after ATP perfusion: contraction, bundles remain stable without contraction (no contraction) or bundles disintegrate as a function of $R_{M:A}$ ($n > 48$ bundles for each data point). Data points obtained within 1 min of ATP perfusion. (*d*) Percent decrease in myosin intensity after the first 45 s of ATP addition. Data shown are mean ± SD ($n = 5$ bundles for each data point).

$R_{M:A}$ increases from 0.64 to 1.9 (*squares*, Fig. 2 *b*). Thus, in the absence of ATP, myosin thick filaments facilitate the formation of cross-linked actin bundles with similar mechanical behaviors over a wide range of myosin densities. Interestingly, bundles fail to form when myosin thick filaments are replaced with similar concentrations of smooth muscle heavy meromyosin, indicating the importance of thick filament architecture for bundle formation (data not shown).

Contraction occurs above a critical myosin concentration

To initiate myosin catalytic activity, Assay Buffer containing ATP is perfused into the chamber. For bundles formed with sparse myosin cross-linking ($R_{M:A} = 0.44$), the addition of 1 mM ATP results in rapid disintegration of a majority of bundles (Fig. 2, *a* and *c*, Movie S3). Concomitantly, ~80% of the myosin dissociates from F-actin (see Fig. 2 *d*) and within 40 s, only F-actin bound to beads remains in the field of view (Fig. 2 *a*). Myosin does not remain bound to individual F-actin, reflecting a weak affinity of thick filaments to F-actin in the presence of ATP (30). This reduced effectiveness of myosin filament cross-links in the presence of ATP is likely the cause of bundle disintegration for bundles with $R_{M:A} < 0.44$ (see Supporting Material).

When $R_{M:A}$ is increased to 0.64, a qualitatively different behavior is observed. After perfusion of 1 mM ATP, ~40% of the myosin detaches (Fig. 2 *d*) but a majority of bundles remain intact several minutes after buffer exchange (Fig. 2, *a* and *c*, Movie S4). The amplitude of the transverse fluctuations cannot be distinguished from those before ATP addition (Fig. 2 *b*) and no change in bundle length is observed. Thus, for $R_{M:A} = 0.64$, bundles remain stable in the presence of ATP but are not contractile.

When $R_{M:A}$ is increased above 0.7, addition of 0.1–1 mM ATP induces a rapid contraction of nearly all bundles. During contraction, bundle contours rapidly change from wavy to straight (Fig. 2 *a*, Movie S5) and contracted bundles are taut with transverse fluctuations below our resolution limit, $<0.002\ \mu m^2$ (Fig. 2 *b*). After becoming taut, ~60% of the bundles rupture ($n = 74$). Contracted bundles that do not rupture remain stable for at least 30 min, the duration of the experiment.

Thus, we find the myosin density within bundles is critical to the nature of bundle remodeling observed in the presence of ATP. When $R_{M:A}$ ~0.64, there is a sharp transition from ATP-induced bundle disintegration to contraction (Fig. 2 *c*). Because a fraction of myosin dissociates from the bundles after ATP addition, a mole ratio that accounts for this decrease, $R^{ATP}_{M:A}$, better reflects the stoichiometry in ATP and we determine that contraction dominates when $R^{ATP}_{M:A} \geq 0.5$.

Contraction occurs in tethered and untethered bundles at rates up to 400 nm/s

To quantify the contraction of bundles with a high density of myosin cross-bridges, $R^{ATP}_{M:A} = 1.4$, we measure their contour length as a function of time (*dashed lines*, Fig. 3, *a* and *c*). After perfusion of Assay Buffer containing ATP, bundle contours rapidly change from wavy to straight and decrease in length by ~5–10% within ~30 s at a maximal rate of ~100 nm/s (Fig. 3, *a* and *b*, Movie S6). When a connection to a neighboring bundle ruptures (*arrow*, Fig. 3 *a*), the change in boundary conditions accommodate an additional contraction of 15% at a rate of ~400 nm/s (Fig. 3, *a* and *b*). During contraction, transient bends within the bundle are often observed (65 s and 75 s, Fig. 3 *a*). After contraction stops, the contours of tethered bundles are straight, taut, and remain stable for longer than 100 s.

After a rupture event, bundles with a free, untethered end are formed (*asterisk*, Fig. 3, *a* and *c*). For untethered bundles, the only effects resisting contraction are the weak viscous drag of the surrounding media and any internal resistive force within the bundle. In comparison to tethered bundles, untethered bundles contract a significantly larger fraction of their original length (~25%, $n = 10$ bundles) with a higher rate of ~400 nm/s (Fig. 3 *d*). Thus, the boundary conditions change the extent and the rate of contraction. This implies that force sustained at the bundle endpoint impacts the extent and rate of bundle contraction.

Force-velocity relationship of reconstituted actomyosin bundles

The elastic polyacrylamide (PAA) gel on which the beads are bound provides a means to measure the tensile force generated during bundle contraction. Forces applied to a bead bound to the top surface induce PAA gel deformations that can be visualized if the gel is sufficiently compliant (31). An effective spring constant determined by the elastic properties of the PAA gel is used to calculate the force from the observed bead displacement (Fig. 4 *a*, Fig. S6). By reducing the shear elastic modulus of the PAA gel from 600 Pa (used in Figs. 1–3) to 54 Pa, we can visualize bead displacement. During contraction of bundles with $R^{ATP}_{M:A} = 1.4$, significant tensile forces are built (Fig. 4, *b* and *c*, Movie S7). In the first 5 s after ATP addition, the force increases to 250 pN as the contraction speed increases from 0 to 120 nm/s (Fig. 4, *c* and *d*). We speculate this may reflect a transient regime during the initiation of myosin mechanochemistry as ATP-containing buffer is perfused. After this initial force buildup, an inverse relationship between contraction speed and force is measured, with the speed decreasing as the forces build to ~600 pN (Fig. 4 *d*, *dashed line*); this presumably reflects the behavior of the system in saturating ATP. After contraction completes, the tensile force of 600 pN is stably maintained for minutes. The force at which bundle contraction stalls is narrowly peaked around 500 pN (Fig. 4 *e*) and no apparent correlation between the stall force and bundle length is observed (Fig. 4 *f*).

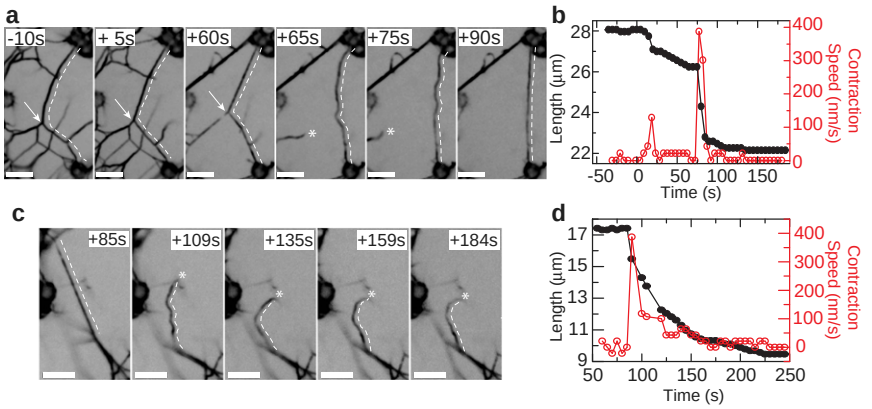

FIGURE 3 Contraction of tethered and untethered bundles. (*a*) Time-lapse series of inverted contrast, OG-myosin images in a contracting bundle with $R^{ATP}_{M:A} = 1.4$. Times are in seconds before (*negative times*) or after (*positive times*) addition of 0.1 mM ATP. Dashed line demarks changing contour of the tethered bundle of interest. A connection to a neighboring bundle breaks between 60 and 65 s (*arrow*), following which contraction of both the untethered bundle (*asterisk*) and tethered bundle (*dashed line*) resume. Scale bar is 5 μm; see Movie S6. (*b*) Contour length (*left axis, solid circles*) and contraction speed (*right axis, open circles*) of the bundle indicated by the dashed line in *a*. (*c*) Time-lapse series of inverted contrast OG-myosin images illustrating the contraction of an untethered bundle following the rupture of a taut bundle 85 s after 1mM ATP addition. Bundle shown contains $R^{ATP}_{M:A} = 1.4$. Asterisk indicates the free bundle end. Scale bar, 5 μm. (*d*) Bundle contour length (*closed circles, left axis*) and contraction speed (*right axis, open circles*) versus time for the contracting untethered bundle shown in (*c*).

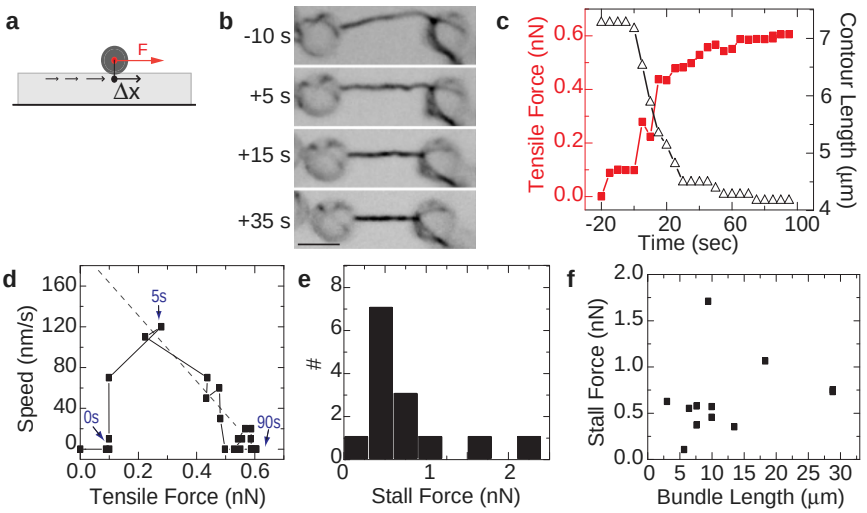

FIGURE 4 Tension is built during contraction of tethered bundles. (*a*) Schematic illustrating how the displacement of a bead bound to the top surface of an elastic hydrogel can be used to determine the forces applied on the bead. A force, F, applied to the surface-bound bead is balanced by the elastic restoring force exerted by the underlying gel, resulting in a bead displacement Δx such that $F = k_{\text{eff}}\,\Delta x$, where k_{eff} is an effective spring constant determined by the gel elastic properties. Further details of this measurement are discussed in Fig. S6. (*b*) Images of OG-myosin (inverted contrast) in a bundle with $R^{\text{ATP}}_{\text{M:A}} = 1.4$. The underlying gel has a shear elastic modulus of 54 Pa. Time = 0 s delineates addition of 1 mM ATP. Scale bar is 5 μm; see Movie S7. (*c*) Tensile force (*left axis, red squares*) and contour length (*right axis, open triangles*) as a function of time for the bundle shown in (*b*). (*d*) Contraction speed versus tensile force for data shown in (*b*). The dashed line approximates the force-velocity relationship observed at long times and high loads. Arrows indicate times = 0 s, 5 s, and 90 s. (*e*) Histogram of maximum tensile force, or stall force, of contractile bundles with $R^{ATP}_{M:A} = 1.4$ and contracted with buffer containing 1 mM ATP. (*f*) Stall forces calculated in (*e*) plotted as a function of initial bundle contour length.

Rate of contraction at low tension is proportional to bundle length

To measure bundle contraction rates in the absence of an external load, we examine untethered bundles contracting after a rupture event. Remarkably, the initial contraction speed strongly correlates with the initial bundle length, showing a linear dependence for both $R^{\text{ATP}}_{\text{M:A}} = 1.4$ and $R^{\text{ATP}}_{\text{M:A}} = 0.49$ (Fig. 5, *a* and *b*). Moreover, zero load contraction velocities are consistent with those obtained by extrapolating the observed inverse force-velocity relationship (*dashed line*, Fig. 4 *d*) to zero load (*open squares*, Fig. 5 *a*). The linear nature of the correlation between contraction speed and bundle length indicates a well-defined contraction speed per unit length of bundle, $\dot{\gamma} = 0.04\ \text{s}^{-1}$ for $R^{\text{ATP}}_{\text{M:A}} = 1.4$. When the myosin density is decreased to $R^{\text{ATP}}_{\text{M:A}} = 0.49$, $\dot{\gamma}$ decreases to $0.02\ \text{s}^{-1}$ (Fig. 5 *b*).

To directly visualize contraction within the bundle, we examine the myosin intensity along the bundle contour (Fig. 5, *c* and *d*). Variations in myosin intensity are observed along the bundle but are <10% of the mean myosin intensity at all times during contraction (Fig. 5, *c* and *d*). During contraction, relative movements of fiduciary marks within the bundle are observed and a variety of local rearrangements ranging from highly contractile to weakly extensile are observed along the bundle length (Fig. 5 *e*). Importantly, no signature of periodic myosin intensities exist during contraction, suggesting a lack of sarcomeric organization within the bundles throughout contraction.

Bundle contraction occurs by several contractile elements connected in series

The observed length-dependent contraction velocity and length-independent stall force are consistent with bundle contraction occurring through a collection of independent contractile elements working in series. In such a model, the rate of bundle contraction is equal to the number of elements N multiplied by the characteristic contraction speed v of a single element. If contractile elements have a length d the number of elements in a bundle of length L is $N = L/d$. As a result, the length-dependent, or telescopic, bundle contraction speed is Lv/d (Fig. 6). Consequently, we expect the contraction rate per unit length observed in Fig. 5, *a* and *b* to be of the order v/d. A natural scale for the contraction speed of a single unit is to be twice that of unloaded smooth muscle myosin, ~400 nm/s (32,33). From this, we estimate d~10 μm for $R^{\text{ATP}}_{\text{M:A}} = 1.4$, approximately twice the F-actin length. As the density of myosin cross-bridges is decreased to $R^{\text{ATP}}_{\text{M:A}} = 0.49$, d increases to ~20 μm. Although difficult to discern from our current data, we speculate that the extent to which any given myosin filament participates as a motor or cross-linker may change over time as the load on it changes during contraction. This adaptation and malleability of contractile elements during contraction has been implicated to explain the contraction of smooth muscle cells (18).

For contractile elements arranged in series, the force generated at the bundle endpoints provides a measure of the force generated by a single element. The contractile force produced by bundles with $R^{\text{ATP}}_{\text{M:A}} = 1.4$ is strongly peaked around ~0.5 nN and the observed load-dependent contraction (Fig. 4 *d*) is consistent with the force-dependent kinetics observed in single molecules of smooth muscle myosin (10). Because the stall force of smooth muscle myosin is ~2 pN (10), this suggests that ~250 motors operate in parallel in each element, corresponding to ~3 myosin thick filaments. Because bundles consist of ~4 F-actin per cross section, we estimate that each pair of F-actin is cross-linked, on average, by 1–3 actively tensed myosin thick filaments.

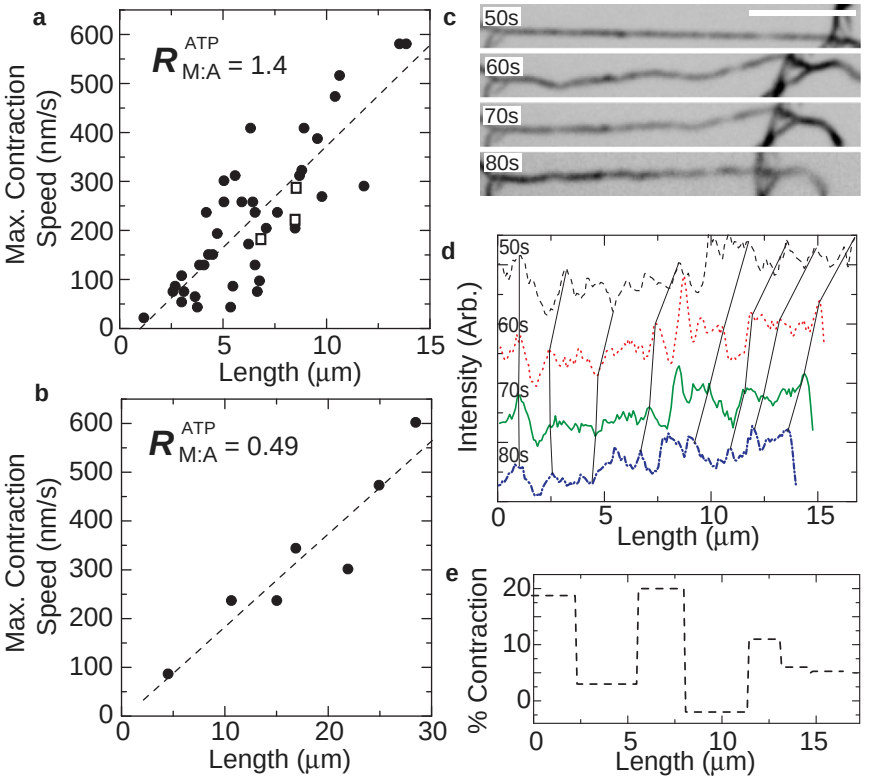

FIGURE 5 Unloaded contraction speed is proportional to bundle length. (*a*) Maximal contraction speed of untethered bundles plotted as a function of initial bundle length for $R^{ATP}_{M:A} = 1.4$ (*solid circles*). Open squares indicate zero-load velocities extrapolated from the inverse force-velocity relationship observed in Fig. 4, *d* (*dashed line*). Dashed line indicates a linear fit to the data with slope $\dot{\gamma} = 0.04\ s^{-1}$ ($R^2 = 0.68$). (*b*) Maximal contraction speed of untethered bundles as a function of bundle length for $R^{ATP}_{M:A} = 0.49$. Dashed lines indicate a linear fit to the data with slope $\dot{\gamma} = 0.02\ s^{-1}$ ($R^2 = 0.87$). (*c*) Inverted contrast images of OG-myosin during the untethered contraction following the rupture of a bundle with $R^{ATP}_{M:A} = 1.4$. Scale bar is 5 μm. (*d*) Line scans of myosin fluorescence intensity along bundle length averaged over a width of 0.5 μm for the images shown in (*c*), showing variations in myosin intensity. Solid black lines indicate guides to observe the movement of fiduciary marks. (*e*) The ratio of the change in distance between two fiduciary marks relative to their initial distance for the fiduciary marks visualized in (*d*) for times between 50 and 60 s. This measure of the percent contraction shows variations in the extent of contraction along the bundle length.

DISCUSSION

Here we have developed a versatile technique to measure the stability and force-generation in bundles consisting of F-actin and myosin thick filaments on cellular length (5–50 μm) and force (0.1–5 nN) scales. We expect this assay will be useful in determining the roles of myosin thick filament architecture, passive cross-linking proteins, and F-actin polymerization dynamics in the contraction of actomyosin bundles. We also expect this could be more generally used to study force-generation in other types of bundles formed by cytoskeletal polymers and accessory proteins.

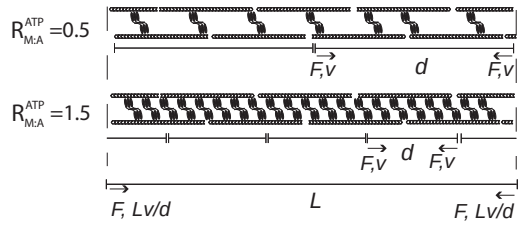

FIGURE 6 Bundle contraction operates as a series of individual contractile units Cartoons illustrating our model of how myosin densities affect the length *d* of contractile elements within the bundle. F-actin (*chevrons*) is bundled through the cross-linking of myosin thick filaments (*black*). A series of contractile elements each contracting with a velocity *v* and stall force *F* will result in the observed length-dependent rate of bundle contraction *Lv/d* and length independent stall force *F*. If the speed of the contractile elements remains unchanged for different myosin densities, then the higher rate of contraction per bundle length observed with high myosin densities (Fig. 5, *a* and *b*) can be explained by a decrease in *d*.

Our data demonstrate the potential of myosin cross-bridges to variably act in both cross-linking and force generating capacities. At low ATP, the high affinity of actomyosin cross-bridges facilitate cross-linking over the entire range of myosin concentrations studied, estimated to be >3 myosin filaments per F-actin (Supporting Material). In the presence of ATP, the low duty ratio of smooth muscle myosin (34) reduces the effectiveness of actomyosin interactions. With a 4% duty ratio (34), each 360 nm long myosin thick filament containing ~200 motor domains will have an average of eight motors bound at any given time (35). The observed decrease in myosin intensity upon ATP perfusion likely reflects the detachment of myosin cross-bridges with suboptimal binding to F-actin (see Supporting Material). We find that low densities of mechanochemically active myosin filaments do not provide sufficient cross-linking to maintain stable bundles. Over a narrow range of 1–4 myosin filaments per F-actin, myosin filaments provide sufficient cross-linking of F-actin to maintain a stable bundle but do not facilitate contraction (Fig. 7). Bundle contraction only occurs at extremely high myosin filament density, more than four thick filaments per F-actin (Fig. 7). We speculate that changing the effective duty ratio of thick filaments, either by altering the duty ratio of individual motors or changing the filament size, would alter the minimum threshold of

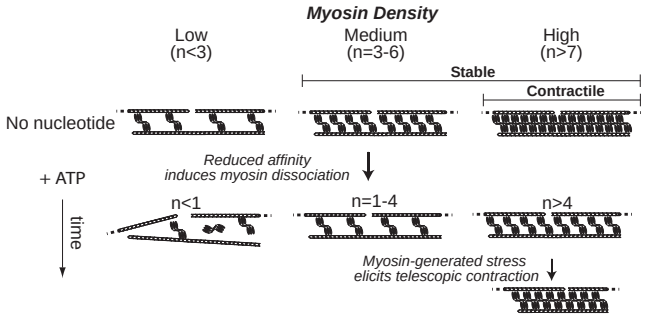

FIGURE 7 Impact of myosin filament density on bundle stability and contraction. The number n of myosin filaments (*black*) per F-actin (*chevrons*) is estimated from measured stoichiometries (Methods in the Supporting Material). In the absence of nucleotide, bundles are stable over a wide range of thick filament density (*top row*). ATP addition reduces the affinity of myosin cross-bridges by initiating motor mechanochemistry (*middle row*). A portion of thick filaments dissociate, leading to loss of bundle structure under low ($n < 1$) myosin densities. Intermediate myosin densities ($n = 1$–4) retain enough cross-linking within bundles to resist ATP-induced bundle disintegration, but no contraction is observed. At the highest myosin densities ($n > 4$), myosin-generated forces lead to bundle contraction (*bottom row*).

motor density required for bundle stabilization and contraction. Furthermore, in the myosin preparation used here, 50% of the regulatory light chains were phosphorylated. Preparations with 100% phosphorylation may yield different results (see Supporting Material).

Our study also shows that a high density of myosin cross-bridges is sufficient to elicit contraction and force generation in mesoscopic actomyosin bundles in the absence of other actin cross-linking or regulatory proteins. Previous in vitro experiments have concluded that passive cross-linking proteins (e.g., α-actinin or filamin) are required to elicit such contraction. This discrepancy can be accounted for by considering that, for previous experiments, $R_{M:A} \leq 0.05$ (23,24). Here, we find that bundle contraction occurs only when $R_{M:A} > 0.75$. We cannot completely exclude the existence of high affinity, dead motors serving as passive cross-linkers in our experiment. However, the limited range of $R_{M:A}$ over which bundling without contractility is observed (Fig. 2 *c*) suggests that high affinity cross-links are rare (see Supporting Material). It will be interesting to explore how the nature of the observed phase diagram is altered in the presence of exogenous actin cross-linking proteins. Because the molar ratio of myosin to actin in smooth muscle cells is 0.2–0.5 (36), actin binding proteins likely play important roles in physiological regulation of contraction.

In striated myofibrils, sarcomeres are the basic contractile element and sarcomeric organization is essential for models of force transmission from the molecular to tissue length scales. However, contractile elements lacking apparent sarcomeric organization have also been proposed for smooth muscle and nonmuscle cells (9,17,19), but an understanding of the molecular or structural requirements of nonsarcomeric contraction has been lacking. Interestingly, the reconstituted bundles shown here lack myosin bands indicative of sarcomeric organization but still form contractile elements that support telescopic contraction of actomyosin bundles. Our data thus offer new, to our knowledge, perspectives on the molecular requirements and physical mechanisms of nonsarcomeric modes of contraction, such as those found in smooth muscle and nonmuscle cells (7,9).

Here, we have shown that actin filaments and mechanochemically competent myosin thick filaments self-organize into contractile elements that can transmit actomyosin forces to cellular length scales. Future work is required to determine whether these interactions can be harnessed to modify F-actin length, sort F-actin polarity, or alter myosin localization, which could result in sarcomere-like organization. We anticipate our study will serve as a starting point for more sophisticated in vitro models that will elucidate mechanisms of force transmission in the actomyosin cytoskeleton and provide insight into the design principles of adaptive biological materials.

SUPPORTING MATERIAL

Seven movies, six figures, Materials and Methods, and text are available at http://www.biophysj.org/biophysj/supplemental/S0006-3495(11)00476-0.

We acknowledge Jim Sellers and Primal de Lanerolle for advice on the purification and handling of smooth muscle myosin; Aaron Dinner, Megan Valentine, and Tom Witten for useful discussions; and Ron Rock and Melanie Norstrom for carefully reading the manuscript. We thank Primal de Lanerolle, Dave Kovar, and Melanie Norstrom for generous gifts of reagents.

This work was funded by a Burroughs Wellcome Career Award, Packard Foundation fellowship and National Institutes of Health Director's Pioneer Award (DP10D00354) to M.L.G. and the University of Chicago Materials Research Science and Engineering Center.

REFERENCES

1. Wozniak, M. A., and C. S. Chen. 2009. Mechanotransduction in development: a growing role for contractility. *Nat. Rev. Mol. Cell Biol.* 10:34–43.
2. Vicente-Manzanares, M., X. Ma, …, A. R. Horwitz. 2009. Non-muscle myosin II takes centre stage in cell adhesion and migration. *Nat. Rev. Mol. Cell Biol.* 10:778–790.
3. Pollard, T. D. 2010. Mechanics of cytokinesis in eukaryotes. *Curr. Opin. Cell Biol.* 22:50–56.
4. Kee, A. J., P. W. Gunning, and E. C. Hardeman. 2009. Diverse roles of the actin cytoskeleton in striated muscle. *J. Muscle Res. Cell Motil.* 30:187–197.
5. Gunst, S. J., and W. Zhang. 2008. Actin cytoskeletal dynamics in smooth muscle: a new paradigm for the regulation of smooth muscle contraction. *Am. J. Physiol. Cell Physiol.* 295:C576–C587.
6. Verkhovsky, A. B., and G. G. Borisy. 1993. Non-sarcomeric mode of myosin II organization in the fibroblast lamellum. *J. Cell Biol.* 123:637–652.
7. Cramer, L. P. 1999. Organization and polarity of actin filament networks in cells: implications for the mechanism of myosin-based cell motility. *Biochem. Soc. Symp.* 65:173–205.
8. Vavylonis, D., J. Q. Wu, …, T. D. Pollard. 2008. Assembly mechanism of the contractile ring for cytokinesis by fission yeast. *Science.* 319:97–100.

9. Herrera, A. M., B. E. McParland, …, C. Y. Seow. 2005. 'Sarcomeres' of smooth muscle: functional characteristics and ultrastructural evidence. *J. Cell Sci.* 118:2381–2392.
10. Veigel, C., J. E. Molloy, …, J. Kendrick-Jones. 2003. Load-dependent kinetics of force production by smooth muscle myosin measured with optical tweezers. *Nat. Cell Biol.* 5:980–986.
11. Cooke, R. 1997. Actomyosin interaction in striated muscle. *Physiol. Rev.* 77:671–697.
12. Szent-Györgyi, A. G. 2004. The early history of the biochemistry of muscle contraction. *J. Gen. Physiol.* 123:631–641.
13. Howard, J. 2001. Mechanics of Motor Proteins and the Cytoskeleton. Sinauer Associates, Sunderland, MA.
14. Cooke, R. 2004. The sliding filament model: 1972–2004. *J. Gen. Physiol.* 123:643–656.
15. Littlefield, R., and V. M. Fowler. 1998. Defining actin filament length in striated muscle: rulers and caps or dynamic stability? *Annu. Rev. Cell Dev. Biol.* 14:487–525.
16. Huxley, H., and J. Hanson. 1954. Changes in the cross-striations of muscle during contraction and stretch and their structural interpretation. *Nature.* 173:973–976.
17. Bement, W. M., and D. G. Capco. 1991. Analysis of inducible contractile rings suggests a role for protein kinase C in embryonic cytokinesis and wound healing. *Cell Motil. Cytoskeleton.* 20:145–157.
18. Kuo, K. H., A. M. Herrera, …, C. Y. Seow. 2003. Structure-function correlation in airway smooth muscle adapted to different lengths. *Am. J. Physiol. Cell Physiol.* 285:C384–C390.
19. Carvalho, A., A. Desai, and K. Oegema. 2009. Structural memory in the contractile ring makes the duration of cytokinesis independent of cell size. *Cell.* 137:926–937.
20. Spicer, S. S. 1951. Gel formation caused by adenosine triphosphate in actomyosin solutions. *J. Biol. Chem.* 190:257–267.
21. Crooks, R., and R. Cooke. 1977. Tension generation by threads of contractile proteins. *J. Gen. Physiol.* 69:37–55.
22. Stendahl, O. I., and T. P. Stossel. 1980. Actin-binding protein amplifies actomyosin contraction, and gelsolin confers calcium control on the direction of contraction. *Biochem. Biophys. Res. Commun.* 92:675–681.
23. Janson, L. W., J. Kolega, and D. L. Taylor. 1991. Modulation of contraction by gelation/solation in a reconstituted motile model. *J. Cell Biol.* 114:1005–1015.
24. Bendix, P. M., G. H. Koenderink, …, D. A. Weitz. 2008. A quantitative analysis of contractility in active cytoskeletal protein networks. *Biophys. J.* 94:3126–3136.
25. Koenderink, G. H., Z. Dogic, …, D. A. Weitz. 2009. An active biopolymer network controlled by molecular motors. *Proc. Natl. Acad. Sci. USA.* 106:15192–15197.
26. Mizuno, D., C. Tardin, …, F. C. Mackintosh. 2007. Nonequilibrium mechanics of active cytoskeletal networks. *Science.* 315:370–373.
27. Altringham, J. D., P. H. Yancey, and I. A. Johnston. 1980. Limitations in the use of actomyosin threads as model contractile systems. *Nature.* 287:338–340.
28. Sellers, J. R. 1985. Mechanism of the phosphorylation-dependent regulation of smooth muscle heavy meromyosin. *J. Biol. Chem.* 260:15815–15819.
29. Peterson, L. J., Z. Rajfur, …, K. Burridge. 2004. Simultaneous stretching and contraction of stress fibers in vivo. *Mol. Biol. Cell.* 15:3497–3508.
30. Lymn, R. W., and E. W. Taylor. 1971. Mechanism of adenosine triphosphate hydrolysis by actomyosin. *Biochemistry.* 10:4617–4624.
31. Sabass, B., M. L. Gardel, …, U. S. Schwarz. 2008. High resolution traction force microscopy based on experimental and computational advances. *Biophys. J.* 94:207–220.
32. Sellers, J. R., J. A. Spudich, and M. P. Sheetz. 1985. Light chain phosphorylation regulates the movement of smooth muscle myosin on actin filaments. *J. Cell Biol.* 101:1897–1902.
33. Warshaw, D. M., J. M. Desrosiers, …, K. M. Trybus. 1990. Smooth muscle myosin cross-bridge interactions modulate actin filament sliding velocity in vitro. *J. Cell Biol.* 111:453–463.
34. Rosenfeld, S. S., J. Xing, …, H. L. Sweeney. 2003. Myosin IIb is unconventionally conventional. *J. Biol. Chem.* 278:27449–27455.
35. Tonino, P., M. Simon, and R. Craig. 2002. Mass determination of native smooth muscle myosin filaments by scanning transmission electron microscopy. *J. Mol. Biol.* 318:999–1007.
36. Gabella, G. 1984. Structural apparatus for force transmission in smooth muscles. *Physiol. Rev.* 64:455–477.